Aggregation and Disaggregation Kinetics of Human Blood Platelets: Part I. Development and Validation of a Population Balance Method

Pin Y. Huang and J. David Hellums
Cox Laboratory for Biomedical Engineering, Rice University, Houston, Texas 77251-1892 USA

ABSTRACT Hydrodynamic shear stress of sufficient intensity is known to cause platelet activation and aggregation and to alter the effects of biochemical platelet agonists and antagonists. In this work, a population balance equation (PBE) model is developed for analysis of platelet aggregation and disaggregation kinetics under the influence of a shear field. The model incorporates both aggregation and disaggregation by splitting and/or erosion mechanisms. This paper, the first of a series of three, deals with the formulation, simplification, and validation of the PBE and with the estimation of parameters involved in the PBE. These population parameters include collision efficiency, void fraction (related to the particle collision diameter), and the breakage rate coefficient. The platelet particle size distribution is determined experimentally, both initially and at some later times. The PBE can then be used to match satisfactorily the observed particle histograms, by appropriate choice of parameters of the model as functions of time, platelet size, and magnitude of physical or chemical stimuli. Besides providing information on adhesive forces and on the rates of aggregation and disaggregation, these parameters infer the physical properties of platelets and platelet aggregates. These properties are of potential value in increasing our understanding of the processes involved in thrombotic disease and/or therapy. A numerical procedure for solving the PBE is validated by application to simple cases for which analytical solutions are available. The model is applied to analysis of experiments, and parameter sensitivity studies are used to order the importance of the parameters and to reduce the complexity of the model. The simplified model is shown to give good agreement with experimental observations.

INTRODUCTION

Platelets play important roles in hemostatic and thrombotic processes. Following blood vessel damage, platelets adhere to the site of the injury and release their granule contents. The materials released stimulate platelet aggregation at the site of injury. The unstable plug formed at the injury site then provides a surface for blood coagulation. In this process, a polymer network is formed on the plug and renders it more stable.

There are many factors that contribute to the activation of platelets. One factor includes the release of biochemicals from an injured blood vessel and from the platelets adhering to the injury site. Other factors are related to the role played by fluid mechanics in a partially occluded vessel. In such vessels, shear stress has been shown to be elevated by as much as 20-fold above the normal level. There is little understanding of the way in which nonbiochemical factors such as hydrodynamic shear stress and platelet-platelet collisions serve to affect platelet activation and aggregation. In this study, the roles played by fluid mechanics in hemostasis and thrombosis are examined. Specifically, we have investigated shear-induced platelet aggregation and disaggregation in the uniform, controlled shear field of a cone-plate viscometer.

This paper is Part I of a three-part series on the use of population balance mathematics to analyze platelet aggregation and disaggregation kinetics. The population balance technique used gives estimates of platelet properties pertinent to aggregation kinetics and to their state of activation. For example, this technique gives a numerical estimate of platelet-platelet binding affinity, a population balance property. The population balance properties so determined offer insights into the dynamic state of platelets as they aggregate and disaggregate. Furthermore, the properties give a concise means of describing the detailed evolution of the particle size distribution over time.

This paper, Part I, details and validates the machinery developed for the determination of the population balance properties as functions of time and magnitude of shear stress. In Part II (1), the method is applied to the analysis of experiments involving platelet aggregation: the aggregation of platelet suspensions subjected to uniform shearing stress in the absence of added agonists. In Part III (2), the method is applied to the analysis of experiments which involve platelet disaggregation: the disaggregation under uniform shearing stress of platelet aggregates previously formed in response to low dosages of added agonists.

Received for publication 25 June 1992 and in final form 11 February 1993.

Address reprint requests to J. D. Hellums.

P. Y. Huang is now with Exxon Production Research, Houston, TX 77252-2189.

This work was supported by the National Institutes of Health under grants 5P50NS23327 and 5R3718584.

0006-3495/93/07/334/10 $2.00

MATERIALS AND METHODS

The population balance equation

Basic equations

The population balance equation (PBE) predicts how the makeup of a collection of particles changes as a result of interaction among the particles, and interactions between particles and the surrounding medium. In the pop-

ulation balance equation, the particle number density function mathematically expresses the makeup of a collection of particles. The argument of the density function can be any particle parameter of interest, for example, the particle volume. Solving the population balance equation determines the number density function as a function of time.

For platelet aggregation in a uniform shear field, an appropriate population balance is the laminar shear coalescence equation (3, 4) given by the first three terms of Eq. 1. The laminar shear coalescence equation is a special case of a general population balance equation in which only aggregation processes are accounted for. The more general case involves both platelet aggregation and disaggregation. Eq. 1 is a population balance equation that includes both coalescence processes and particle breakup due to splitting. The last two terms pertain to breakup or disaggregation. The breakage terms in Eq. 1 are in the form first suggested by Melzak (5, 6) and applied by Valentas et al. (7, 8), in their studies of droplet breakup, and by Pandya and Spielman (9, 10) in their studies on floc breakage.

$$\frac{\partial n(v,t)}{\partial t} = \int_{v_s}^{v/2} k_G(w, v-w)\, n(w,t)\, n(v-w,t)\, dw, - \int_{v_s}^{\infty} k_G(w,v)\, n(w,t)\, n(v,t)\, dw + \int_{v}^{\infty} n(w,t)\, \gamma(w)\, g(w)\, p_s(w,v)\, dw - n(v,t)\, g(v) \quad (1)$$

where $0 \le t < \infty$, $v_s \le v < \infty$.

The domain of Eq. 1 encompasses all times and all particle volumes above the smallest particles, v_s, present initially. The terms v and w represent particle volumes. t represents the time, and $n(v,t)dv$ represents the differential number of particles in the size range $(v, v + dv)$/unit suspension volume. $k_G(w,v)$ is the collision frequency factor, called the laminar shear coalescence kernel. The coalescence kernel, $k_G(w,v)$, is introduced by assuming that the average number of collisions between particles of volume v to $v + dv$ and those of volume w to $w + dw$, is $n(w,t)n(v,t)k_G(w,v)dvdwdt$ during the time interval t to $t + dt$. The coalescence kernel is a function of the physical properties of the medium, the governing coagulation processes, and particle sizes. Smoluchowski (11) derived the following expression for the laminar shear coalescence kernel by assuming rectilinear approach of spherical particles,

$$k(w,v) = \frac{G}{\pi}[w^{1/3} + v^{1/3}]^3 \quad (2)$$

where G is the shear rate.

The term $\gamma(w)$ is the number of daughter fragments formed from the breakup of a parent particle of volume w. The breakage rate, $g(w)$, is the fraction of particles with volume between w and $w + dw$, disappearing through breakage/unit time. In a manner analogous to the definition of $k_G(w, v)$, the breakup kernel, $\gamma(w)g(w)p_s(w,v)$, represents that $\gamma(w)g(w)p_s(w,v)$-$n(w,t)dvdwdt$ is the average number of particles of volume v to $v + dv$ created from the breakup of parent particles of volume w to $w + dw$ during the interval t to $t + dt$. The initial particle size distribution, $n(v,0)$, and both kernels must be specified for the problem to be fully posed.

The term on the left-hand side of Eq. 1 represents the rate of accumulation of particles with volume v. The first integral on the right-hand side describes the rate of formation of particles with volume v by collision and binding together of two particles whose volumes add up to v. The second integral represents the rate of disappearance of particles with volume v by their collision and binding with a particle of any volume. The third integral accounts for the production of particles with volume v in the breakup process of particles with volume w $(v \le w < \infty)$. The last term accounts for the disappearance of particles with volume v due to their breakup into particles with volume w $(0 \le w \le v)$. The equation is formulated in such a manner that total mass or volume of the particles is conserved,

$$\int_0^{\infty} n(v,t)\, v\, dv = \text{constant} = N_0 v_0 \quad (3)$$

where N_o is the initial total number concentration of particles, and v_o is the initial mean volume of the particles.

The breakage or disaggregation terms given above in Eq. 1 are based on a splitting mechanism. That is, each particle splits into a specified number of daughter particles, γ. An alternative or supplementary formulation is that of a continuous surface erosion of particles from an aggregate (9, 10). The alternate form was tested, and, as will be shown, was found to be less successful than the splitting model in the particular application studied here. Thus, the detailed formulation of the erosion model is given only in the appendix of this paper. More detail on all equations discussed is given elsewhere (12).

Breakage rate expressions

Proposed mechanisms for the splitting frequency, $g(w)$, and daughter fragment distribution, $p_s(w,v)$, vary widely, depending upon the specific fragmentation process of interest. A simple power-law model for breakage rate or splitting frequency is often seen, particularly in comminution literature (13). Intuitively, $g(w)$ is expected to be an increasing function of parent particle size, w, because large aggregates split more readily than small ones. For such a mechanism, the splitting frequency is sometimes taken to be given by the following.

$$g(w) = k_1 w^m \quad (4)$$

This form is equivalent to that used by Valentas et al. (7, 8), Ramkrishna and Borwanker (14), Ray and Hogg (15), and Pandya and Spielman (9, 10). k_1 and m are parameters that depend on the experimental conditions.

Various forms of the distribution kernel, $p_s(w,v)$, are used by different prior workers. Peterson (16) has given a table containing distribution functions for several particle breakup processes. The breakage events are the results of several factors, including shear forces, interparticle forces, and aggregate morphology. For an aggregate of size w, the sizes of daughter fragments are distributed about a mean value, $\bar{w}$. Following Valentas et al. (7, 8) and Pandya and Spielman (9), the breakage may be considered to be the composite of a large number of independently distributed events that individually contribute only slightly to the outcome of distribution. These workers have suggested that $p_s(w,v)$ could be approximated by a normal density function given by Eq. 5.

$$p_s(w,v) = \frac{1}{\sqrt{2\pi}\sigma} \exp\left(\frac{-(v-\bar{w})^2}{2\sigma^2}\right) \quad (5)$$

As discussed by Valentas et al. (7, 8) and Pandya and Spielman (9, 10), the normal density function cannot represent a distribution of particle sizes with complete precision, because it admits negative values of particle volume, i.e., the values of the normal density function range from $-\infty$ to $+\infty$. However, the variance can be chosen so that the density lies almost entirely within the mass range 0 to v. The probability that v falls outside $\bar{w} \pm c\sigma$ is given by

$$p' = \int_{-\infty}^{\bar{w}-c\sigma} p(w,v)\, dv + \int_{\bar{w}+c\sigma}^{\infty} p(w,v)\, dv = 1 - \left(\frac{2}{\sqrt{\pi}}\right) \int_0^{c/\sqrt{2}} \exp(-z^2)\, dz. \quad (6)$$

Valentas et al. (7, 8) have shown that, for $c = 2$, $p' = 0.0455$ and, for $c = 3$, $p' = 0.0037$. So σ can be expressed in terms of $\bar{w}w$ to obtain the desired accuracy. If v is to lie between $\bar{w} \pm c\sigma$, then $\sigma = \bar{w}/c = \bar{w}/c\gamma$, where γ is the number of daughter fragments. Following Pandya and Spielman

(9, 10), the standard deviation is assumed to have the form

$$\sigma(w) = k_3 w^q \tag{7}$$

where k_3 and q are parameters specific to a given system.

Since naturally occurring populations are frequently skewed, an alternative representation of such a distribution is the logarithmic-normal distribution. In this work, normal and logarithmic-normal distributions were found to give equally good agreement with the experimental observations. The normal distribution was used for all results presented here.

Pandya and Spielman (9) found that the number of daughter fragments upon splitting increased as the size of the parent particle increased, and suggested the following expression for the number of daughter fragments, γ,

$$\gamma - 2 = k_2 \left(\frac{w}{v_0}\right)^p \tag{8}$$

where k_2 and p are parameters specific to a given system. The mean daughter volume upon breakage from a parent particle of volume w is then given as follows.

$$\bar{w} = \frac{w}{2 + k_2 \left(\frac{w}{V_0}\right)^p} \tag{9}$$

Dimensionless variables

The PBE is made dimensionless by the following expressions:

$$x = v/v_0 \tag{10}$$

$$y = w/v_0 \tag{11}$$

$$n(x,t) = v_0 n(v,t)/N_0 \tag{12}$$

$$\tau = (G v_0/\pi) N_0 t \tag{13}$$

$$k_G(x,y) = k_G(v,w)/(G v_0/\pi) \tag{14}$$

$$\gamma(y) g(y) p_s(x,y) = \gamma(w) g(w) p_s(w,v)(\pi/G N_0) \tag{15}$$

Equations 10 and 11 define the dimensionless particle volumes, x and y. Equation 12 defines the dimensionless number density. Equation 13 defines dimensionless time. Note that $n(x,t)$ and $n(v,t)$ are different functions, not the same function with different arguments. Equations 14 to 15 specify the dimensionless laminar shear coalescence kernel and breakage kernel, respectively. Introducing the definitions and simplifying the PBE yields a dimensionless form of the population equation,

$$\frac{\partial n(x,\tau)}{\partial \tau} = \int_{x_s}^{x/2} k_G(y, x-y)\, n(y,\tau)\, n(x-y,\tau)\, dy - \int_{x_s}^{\infty} k_G(y,x)\, n(x,\tau)\, n(y,\tau)\, dy + \int_{x}^{\infty} n(y,\tau)\, \gamma(y)\, g(y)\, p_s(y,x)\, dy - n(x,\tau)\, g(x) \tag{16}$$

where $x_s \le x < \infty$ and $0 \le t < \infty$.

Although in dimensionless form, $n(x,\tau)$ remains awkward to manipulate because x ranges over several orders of magnitude. Replacing x with a logarithmic scale, $L(x)$, compresses the numerical range to a more manageable limit (4, 17). The definition of the logarithmic scale is

$$L(x) = \ln(x/x_s)/\ln 2. \tag{17}$$

The sequence $x = x_s, 2x_s, 4x_s, 8x_s, 16x_s$, now corresponds to $L = 0, 1, 2, 3, 4 \ldots$. $n(L,\tau)$ relates to $n(x,\tau)$ by the following expression,

$$n(L,\tau) = x n(x,\tau) \ln 2. \tag{18}$$

Introduction of population balance parameters

The laminar shear coalescence kernel contains assumptions that are inappropriate for platelet aggregation. A key assumption is that spherical particles coalesce to form larger spherical particles. Platelets, however, are oblate ellipsoids with an average aspect ratio (18) of 3:1. Using electron micrographs, Born and Hume (19) have shown that platelet aggregates take on irregular shapes and contain significant void volume. The laminar shear coalescence kernel also assumes all particle collisions result in the binding together of the involved particles. Experimental evidence by Karino and Goldsmith (20), Chang and Robertson (21), and Bell and Goldsmith (22) suggest that only a small fraction of the collisions result in the binding together of the involved particles. Belval and Hellums (4) corrected these assumptions underlying the laminar shear coalescence kernel by introducing two population balance properties: the collision efficiency, ϵ; and the particle void fraction, ϕ. They proposed and tested several modified coalescence kernels containing different population balance properties designed to relax questionable restrictions in Eq. 2. Among those tested, they found the following expression gave the best correlation with experimental data on shear-induced platelet aggregation,

$$k_G(x,y) = \epsilon(\tau)\left[\left(\frac{x}{1-\phi(x)}\right)^{1/3} + \left(\frac{y}{1-\phi(y)}\right)^{1/3}\right]^3$$

where

$$\phi(x) = \begin{cases} 0, & x < 2 \\ \phi_a, & x \ge 2 \end{cases} \tag{19}$$

and

$$0 \le \epsilon(\tau) \le 1, \qquad 0 \le \phi(x) < 1.$$

Here ϕ_a is a parameter (not a function of x). Equation 19 regards the particles with dimensionless particle volumes less than $x = 2.0$ as singlets and particles with dimensionless particle volumes above $x = 2.0$ as aggregates. The collision efficiency, $\epsilon(\tau)$, is the fraction of the collisions which result in binding together of the involved particles. The particle void volume, $\phi(x)$, replaces "packed" particle volume x, with "total" particle volume, $x/(1-\phi(x))$, as an argument of the coalescence kernel. By enclosing more void volume, hypothetical spherical aggregates achieve a higher collision diameter in an effort to simulate the actual irregular particles, which have an expanded collision diameter. The term "void fraction" for $\phi(x)$ is misleading in that seems to suggest that $\phi(x)$ is the porosity of aggregates. However, it is not the porosity, because the aggregates do not form a spherical structure. It is a correction factor for achieving the same collision diameter as the irregular particles. The issue of aggregate porosity will be addressed later.

The use of a step function in $\phi(x)$ tends to give rise to a rapid change in the size distribution near $x = 2$. Therefore, a linear form of $\phi(x)$ was also investigated:

$$\phi(x) = \begin{cases} 0, & x < 2 \\ \phi_a\left(\frac{x-2}{x_L - 2}\right), & 2 \le x < x \\ \phi_a, & x \ge x_L \end{cases} \tag{20}$$

where x_L and ϕ_a are the parameters which may be adjusted to fix the slope and upper limit of the linear function. The step function and linear function forms of $\phi(x)$ were tested in the pilot studies. The linear function gives a smoother change in the size distribution near $x = 2$; however, it was less

successful in predicting the rate of disappearance of singlets and the formation of intermediate size aggregates under the conditions studied. Therefore, a step function was used for $\phi(x)$ in the results presented here, except where otherwise noted.

For the breakage rate, irregular aggregates are expected to break more readily than the more nearly spherical aggregates. Thus, the breakage rate is modified to have the following form.

$$g(x) = k_1\left(\frac{x}{1-\phi}\right)^m \tag{21}$$

In some cases we studied the use of Lu and Spielman's notion of a minimum splitting size, x_{ss} (23) as follows.

$$g(x) = \begin{cases} k_1 x^m, & \text{for } x > x_{ss} \\ 0, & \text{for } x \le x_{ss} \end{cases} \tag{22}$$

In this expression, we defined k_1 as being different for single particles than for aggregates (for singlets or $x < 2$, $k_1 = k_{10}$ and for aggregates $k_1 = k_{10}/(1-\phi)$). Singlet particles should be resistant to splitting, and preliminary work confirmed that this form of $g(x)$ gives better agreement with experimental volume density distributions, especially in disaggregation experiments.

The numerical method

Determination of population balance parameters from experimental observations

The PBE and the auxiliary equations contain a number of parameters. With all the parameters specified, the PBE can be integrated. Starting with a given initial particle size distribution, $n_{exp}(L(x),0)$, we obtain a size distribution at a later time, τ, $n_{cal}(L(x),\tau)$. Here $L(x)$ is the dimensionless logarithmic particle volume scale defined in Eq. 17. Our goal is to solve the inverse problem of characterizing the parameters in the auxiliary functions by use of experimentally determined particle size distributions. The population balance equation is numerically integrated by the use of a spline collocation method (4). A natural cubic spline approximates the number density curve $n(L(x))$. The approximation exactly satisfies the population equation at certain points, called collocation points. In this case, the collocation points are knot points connecting the piecewise cubics that comprise the natural cubic spline. The parameters are searched for by a nonlinear least squares method for the values of parameters that best fit the experimental data, $n_{exp}(L(x))$. In other words, one seeks the values of ϵ, ϕ, k_1, etc. that minimize an objective function. In the work described here we minimized an objective function expressed in terms of a volume density distribution $v(L(x))$ rather than number density $n(L(x))$. The two distributions are related as outlined below

$$v(x) = xn(x) \tag{23}$$

or, in terms of $L(x)$,

$$v[L(x)] = x_s 2^L n[L(x)]. \tag{24}$$

The choice of objective function gives weight to aggregates in proportion to their size

$$F(\epsilon, \phi, k_1, \gamma, \ldots) = \sum_i \frac{[v_{cal}(L_i)/h_i - v_{exp}(L_i)]^2}{[v_{exp}(L_i)]^2} \tag{25}$$

where v_{cal} and v_{exp} are calculated and experimentally observed volume densities. The use of the porosity correction factors, h_i, is discussed in the next section. The summation in Eq. 25 is over the aggregate size histogram acquired experimentally.

A schematic diagram for the parameter estimation procedure is given elsewhere (12). The function F is minimized using a computer subroutine based on the nonlinear simplex algorithm of Nelder and Meads (24). A nongradient-based minimization algorithm (a region elimination method) is chosen over a gradient-based method to avoid excessive amounts of computation required to evaluate the objective function. One disadvantage of the algorithm is that the optimum values for the parameters from the search are not guaranteed to represent a global minimum. Solutions starting from different initial conditions gave equivalent results, suggesting that the minima are global. To avoid scaling problems, all variables are scaled to comparable magnitudes.

Correction for aggregate porosity

Particle aggregation and breakup are assumed in the PBE calculations to be volume-conserving processes. Yet, due to liquid trapping and experimental artifacts (12), experimentally observed total volumes for aggregated samples are greater than for the unaggregated control sample by 10–50%. To account for these differences, the volume of aggregates from the model was increased by a factor h. This factor h is the ratio of net volume to the gross volume (the apparent "porosity" of an aggregate is $1 - h$). The net volume is intended to correspond to the volume of solid mass. The gross volume is intended to correspond to the volume of solid mass plus the void spaces that are occupied by the fixative or trapped plasma. An empirical expression for h is given by Latimer (25),

$$\begin{aligned} h &= 1 && \text{for} \quad x \le 2 \\ h &= H + (1-H)/(x-1)^{1/2} && \text{for} \quad x > 2 \end{aligned} \tag{26}$$

where H is the limiting value of h for large aggregates, determined from experimental observations.

For aggregates larger than a doublet, the volume of aggregates is increased by the factor h which depends on the number of particles in the assemblage. From the cell packing studies and platelet studies of Born and Hume (19), the value of H is observed to vary between 0.6 and 0.8 for platelet aggregates. In the present work, numerical values of H were determined by an iterative method using experimentally determined particle size histograms, so that the total volume observed experimentally is equal to the calculated volume. The iterative procedures lead to a calculated total volume as given by Eq. 27 as follows.

$$v_{tot} = \sum_i \left(\frac{v_{cal}(L_i(x),\tau)}{h_i}\right) \tag{27}$$

The value of H is found by iterations to yield a calculated total volume, Eq. 26, in agreement with the experimental determination. In this way, the experimental size distribution can be compared to a calculated size distribution that has the same total volume.

For shear-induced platelet aggregation, the values of H obtained from this study range from 0.55 to 0.9; this range is consistent with findings of prior workers. For the disaggregation studies, in some cases a decrease was observed in the total volume of aggregates following breakage. In the cases where the total apparent volume is lowered following breakup, the values of H may exceed one to correct for the decrease in total volume. This decrease in total volume following disaggregation can be explained by the fact that daughter fragments contain less void space than large aggregates.

Validation of numerical methods

For the coalescence equation, the numerical technique is validated by comparing its solution with exact solutions for simple forms of kernels. Melzak (5, 6) has shown that analytical solutions are possible for coalescence kernels of the form

$$k_G(x,y) = A + B(x+y) + C(xy) \tag{28}$$

where A, B, and C are constants. Scott (26) derived analytical solutions for various forms of initial condition including Dirac Delta functions and gamma functions. Detailed derivations are given by Scott (26) and Drake (3). Analytical solutions for an initial condition given by a gamma function, are examined in this study for two special cases of the coalescence kernel,

$k_G(x,y)$. Case 1 is for a constant kernel: $A = 1$, and $B = C = 0$. Case 2 is for the variable kernel: $B = 1$, and $A = C = 0$.

Case 1 For the initial condition $n(x,0)$ given by gamma function and $k_G(x,y) = 1$:

$$n(x,0) = \frac{(\vartheta + 1)^{\vartheta+1} x^{\vartheta} e^{-(\vartheta+1)x}}{\vartheta!} \tag{29}$$

$$n(x,P) = P^2(\vartheta + 1)^{(\vartheta+1)} e^{-(\vartheta+1)x} \sum_{j=0}^{\infty} \frac{(\vartheta + 1)^{j(\vartheta+1)}(1 - P)^j x^{\vartheta+j(\vartheta+1)}}{\Gamma[(j + 1)(\vartheta + 1)]} \tag{30}$$

where P is the total dimensionless population expressed as the total number of particles at time, τ, divided by the total number at time 0.

Case 2 For the same initial condition and $k_G(x,y) = x + y$:

$$n(x,P) = Pe^{-(\vartheta+2-P)x} \sum_{j=0}^{\infty} \frac{(\vartheta + 1)^{(j+1)(\vartheta+1)}(1 - P)^j x^{\vartheta+j(\vartheta+2)}}{(j + 1)!\,\Gamma[(j + 1)(\vartheta + 1)]} \tag{31}$$

In these equations is an integer which alters the character of the function (taken to be 6 in this work). In Eqs. 30 and 31, the gamma function is approximated by Stirling's asymptotic series (27).

Numerical results from solving Eq. 16 were compared with the analytical solutions given by Eqs. 30 and 31. The solutions in each case used the initial distribution of Eq. 31 and were carried out to the same final total particle population, P. Results were expressed in both volume and number density form for four different particle populations, $P = 0.9, 0.8, 0.58$, and 0.24. Fig. 1 presents a comparison between the analytical solution for the coalescence equation with those of numerical solutions for $P = 0.24$. In this figure, the abscissa is the dimensionless logarithmic particle size, $L(x)$, and the ordinate is the volume density function for the particle population. The open triangles in the figure are calculated by using the analytical solution given by Eqs. 30 and 31. The solutions generated by the numerical method are given by open squares.

Plotted in the number density form (not shown), the two solutions are indistinguishable on the scales of the figures. In the volume density form, where one places greater emphasis on the large aggregates, we also see very good agreement. The slight discrepancy in the volume density at $L = 10$ in Fig. 1 is likely to be due to error in evaluating the infinite series for the analytical solutions. In all comparisons, the square fraction error between the numerical solution, f, and the exact solution, y, $\Sigma(f_i - y_i)^2/\Sigma y_i^2$, is less than 3×10^{-5}. The subscript i denotes a numerical node point. The maximum error expressed as, $(\max \mid f_i - y_i \mid)/(\max \mid y_i \mid)$ is less than 1×10^{-2}. Total volume was followed to test for conservation as an indicator of numerical error. Volume was conserved to within 1.3% in all cases. More detail on the comparison is available (12).

Studies on form and parameter sensitivity

Comparisons of size distributions for various forms of $k_G(x,y)$

Analytical solutions to the PBE are known only for certain simplified forms of the coalescence kernel, and only for certain initial size distributions such as that described by a gamma function. The gamma function is only an inexact approximation of a platelet size distribution. However, it is useful for pilot studies to compare various forms of the coalescence kernel.

In this section, the applicability of simpler forms of the coalescence kernel for describing platelet aggregation in laminar shear flow is considered. For an initial condition, $n(x,0)$, given by a gamma function, the size distributions generated by analytical solutions for $k_G(x,y) = 1$ and $k_G(x,y) = (x + y)$ are compared with the numerical solution for the laminar shear kernel, $k_G(x,y) = (x^{1/3} + y^{1/3})^3$. These kernels are compared on the basis of the same initial condition, and the same final total particle population, P. Comparison studies were carried out in terms of both the volume and number density functions, for four different particle populations, $P =$ 0.9, 0.8, 0.58, and 0.24. Fig. 2 gives comparisons among three models for $P = 0.24$ in terms of the volume density distribution. The computed curve for the initial condition (open circles) is generated by the use of $\upsilon = 6$ in the gamma distribution. The open triangles in Fig. 2 are analytical solutions for $k_G(x,y) = (x + y)$. The solutions generated by the numerical method for $k_G(x,y) = (x^{1/3} + y^{1/3})^3$ are given by the open squares, and solutions for $k_G(x,y) = 1$ are given by asterisks.

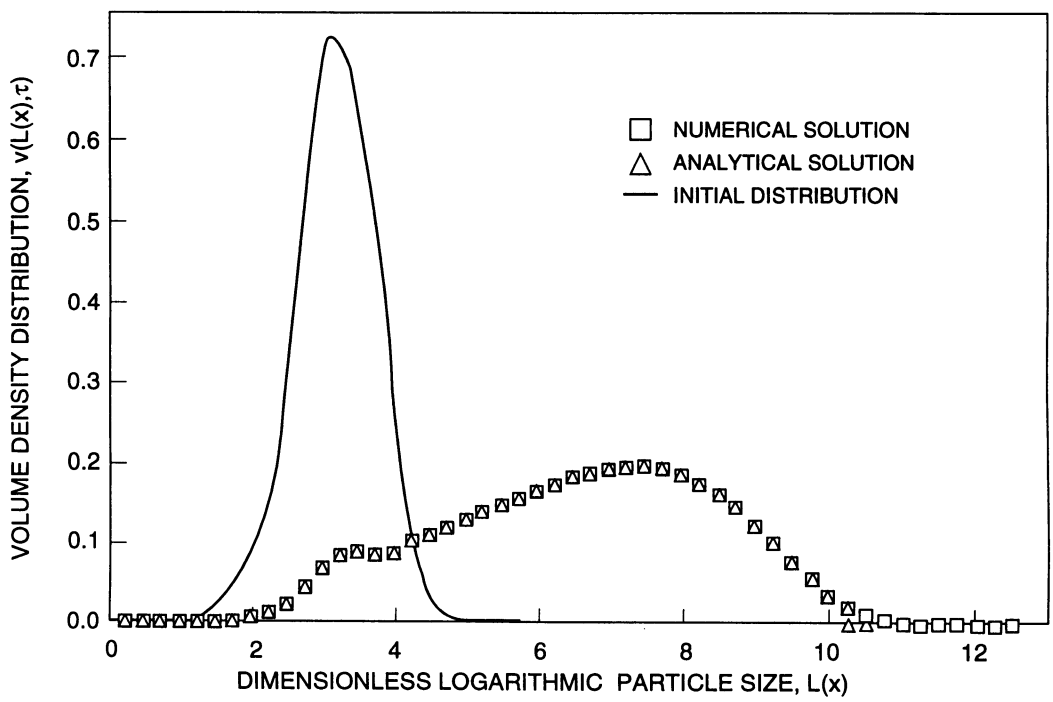

FIGURE 1 Comparison of the analytical solution with the numerical solution in volume density form for a Golovin kernel $k_G(x,y) = x + y$. The two solutions are for the same initial volume density distribution given by the gamma function of Eq. 29, and for the same final total particle population, $P = 0.24$. As indicated, the numerical and analytical solutions are indistinguishable over almost the entire range of comparison.

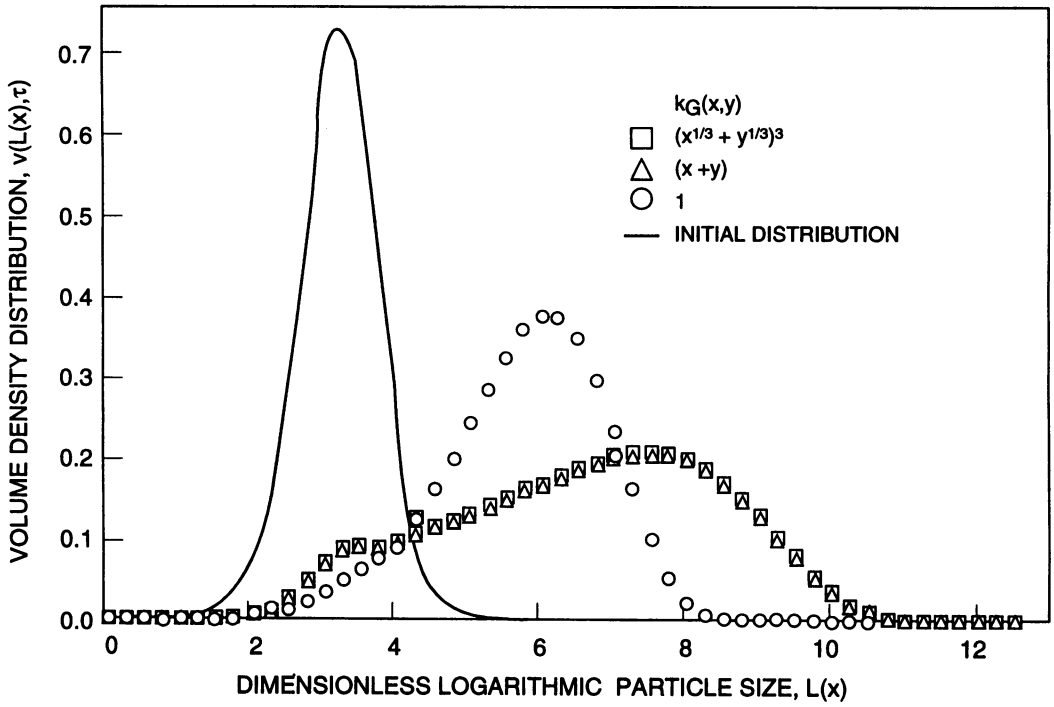

FIGURE 2 Comparison of particle size distributions in volume density form generated using three different kernels. The comparisons are based on the same initial volume density distribution given by the gamma function of Eq. 29 and for the same final particle population, $p = 0.24$.

Examination of the number density plot (not shown here), shows that the constant kernel, $k_G(x,y) = 1$, overestimates the number of small aggregates remaining in the suspension for $P < 0.8$. The differences among these kernels are emphasized when the same information is constructed in volume density form as shown in Fig. 2. The constant kernel overestimates the number of small to mid-size aggregates and underestimates the number of large aggregates in all cases shown. It is clear that the constant kernel is not adequate for characterizing platelet aggregation. In contrast, the kernel, $k_G(x,y) = (x + y)$, seems to give good agreement at all stages of aggregation with the unmodified laminar shear kernel. The maximum normalized residual sum of error squared is less than 10^{-2} in the worst case considered, $P = 0.24$.

The numerical method of Belval and Hellums (4) has the advantage that it allows one to work with a realistic coalescence kernel for all time stages, but at the cost of computation time. Alternatively, one could modify the Golovin kernel, $k_G = (x + y)$, where the analytical solution is known, to account for a collision efficiency and a void fraction as in Eq. 19. Since the Golovin kernel is linear in x and y, the collision efficiency and void fraction can be grouped together in the form $(\epsilon/(1 - \phi))(x + y) = \epsilon'(x + y)$ where ϵ' is $\epsilon/(1 - \phi)$, the modified collision efficiency. This grouping simplifies the problem by reducing the number of parameters. This finding suggests that $\epsilon/(1 - \phi)$ be used as a correlating device rather than the individual parameters ϵ and ϕ. This relationship would be correct if the coalescence kernel were $k_G(x,y) = (x + y)$, and if ϕ were constant. It can only be an approximation, since the most successful form of ϕ is a function of x, as shown in Eq. 19. To test the applicability of the approximation, particle size distributions were generated with two different sets of ϵ and ϕ, which are related by the following expression

$$\left(\frac{\epsilon_1}{1 - \phi_1}\right) = \left(\frac{\epsilon_2}{1 - \phi_2}\right) \tag{32}$$

where $\epsilon_2 = 2\epsilon_1$, and $\phi_2 = 2\phi_1 - 1$. The calculations used the laminar shear kernel (Eq. 19). Since the ratio $\epsilon/(1 - \phi)$ is the same for the two cases, if the expression suggested above serves as a correlating device, then the two particle size distributions generated should be similar. Comparison of the two distributions given in Fig. 3 shows that the results for the two cases are in excellent qualitative agreement, and good but not exact quantitative agreement. The mean square error defined by Eq. 25 is 0.024.

Shear-induced platelet aggregation

Equation 1 and the auxiliary functions were applied to analyze aggregation kinetic data in a laminar shear field. The experimental procedure and more detailed results are described in the second paper of this series (1). There are a total of eight population parameters in this model. Two parameters (ϕ_a and ϵ) come from the coalescence kernel, and six parameters (k_1, m, γ, σ, p, and q) come from the breakage kernel. In the shear-induced platelet aggregation studies, the only breakage mechanism taken into account is that of splitting. To reduce the computation time necessary for the determination of parameters, and to make the problem more tractable, parameter sensitivity analyses were carried out to determine which parameters are most important. Values for parameters which were found to be insensitive are taken from literature. Parameters p of Eq. 8 and q of Eq. 7 were shown by Pandya and Spielman (9) to be unimportant in their applications, and they were taken to be zero in the sensitivity studies. Based on this prior work, we took the breakage due to splitting to be proportional to $v^{1/3}$, and the average number of daughter fragments, γ, to be 2.5. The variance, σ, in the normal distribution was set at 0.25 so that the probability of having negative volume is less than 0.001.

In the sensitivity studies, the first step was to use the simplex algorithm by Nelder and Meads (24) to search for the optimum values for collision efficiency, ϵ, void fraction, ϕ_a, and breakage rate constant, k_1. Sensitivity was then calculated for various population parameters using Eq. 33 as follows.

$$\text{Sensitivity} = \left(\frac{(\partial F/\partial \xi)}{(F/\xi)}\right) \cong \left(\frac{(\Delta F/\Delta \xi)}{(F/\xi)}\right). \tag{33}$$

In Eq. 33, F is the objective function (Eq. 25) and ξ is the estimate of the parameter near the minimum of F. The partial derivative is approximated by a centered difference with $\Delta x = 0.1x$. Typical sensitivity values for ϕ_a,

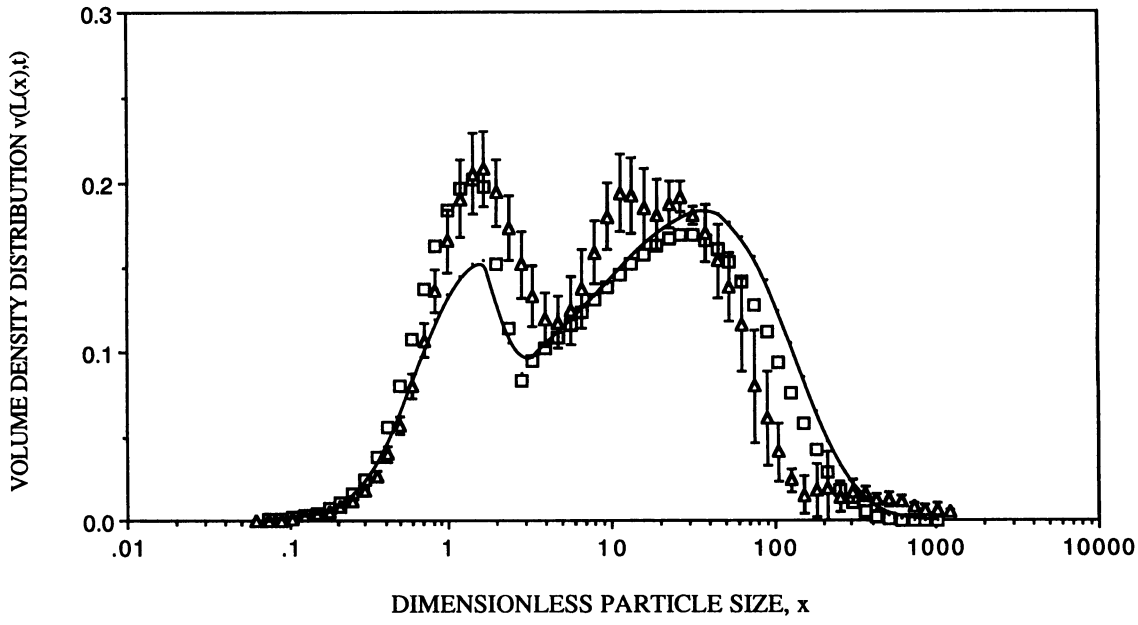

FIGURE 3 Comparison of the volume density histograms generated by sets of parameters such that $\epsilon_1/(1 - \phi_1) = \epsilon_2/(1 - \phi_2)$, where $\epsilon_2 = 2\epsilon_1$, and $\phi_2 = 2\phi_1 - 1$; (△) experimental observed histogram for PRP following 100-s exposure to $G = 5400\ s^{-1}$; (□) pure coalescence solution with $\epsilon_1 = 2.26 \times 10^{-4}$ and $\phi_1 = 0.878$; and (–) pure coalescence solution with $\epsilon_1 = 5.52 \times 10^{-4}$ and $\phi_1 = 0.75$. All histograms have the same particle volume and time. The experimental points represent the mean ± SE (n = 3–5).

ϵ, k_1, m, γ, and σ were found to be 27, 2.7, 0.5, 1.5, 1.0, and 0.023, respectively, for shear-induced aggregation. In all cases, population parameters ϕ_a and ϵ were found to be the most sensitive. Values for m and γ appear to be somewhat more sensitive than the breakage rate constant, k_1. However, the values for m and γ were fixed and may not be the optimum values. Studies where the simplex algorithm was used to search for all five parameters showed that the three breakage parameters (m, γ, and k_1) are equally sensitive, and consistently less sensitive than that of ϕ_a and ϵ. In most of the subsequent shear-induced platelet aggregation studies, estimates for the parameters ϵ, ϕ_a, and k_1 were searched for using the optimization routine with $m = 1/3$ and $\gamma = 2.5$.

Case studies were carried out to establish the effects of ϕ_a, ϵ, k_1, m, and γ on the calculated particle size distribution. In Fig. 4, the computed final condition with optimized values of the parameters is given by open triangles. Solutions for a 10% increase and decrease in ϕ_a are given by plus signs and open circles. The experimental observation for the aggregated sample is given by the open squares. A 10% increase (+) in the values of ϕ_a results in a drastic decrease in the singlet and small aggregate peak and a shift of the large aggregate peak to the right as shown by the arrows in Fig. 4. Repeated calculation with a 10% decrease in the estimate for ϕ_a reverses the trend by increasing the small aggregate peak and shifting large aggregates to the left. Similar studies on the effect of ϵ, the collision efficiency, gave very similar patterns of changes. In contrast, no noticeable change was observed for 10% changes in the breakage parameters k_1, m, and γ. Increasing k_1 by an order of magnitude was required to result in an analogous increase in the singlet peak and shift of the large aggregate peak. Similarly, decreasing k_1 by an order of magnitude resulted in a decrease in the singlet peak and a shifting of the second peak toward larger particle sizes. However, further decreases in the value of k_1 produced no detectable changes in the particle size distribution. Therefore, the breakage terms in Eq. 1 are of little consequence in the determination of the size distribution for shear-induced aggregation. For practical purposes, the phenomena may be treated as an irreversible coalescence.

Disaggregation in a shear field

Other parameter sensitivity studies were carried out for cases in which disaggregation was known to be important: the disaggregation in the shear field of platelet aggregates previously formed in response to low dosage adenosine diphosphate (ADP) addition to platelet suspensions. The experimental procedure and additional results are given in the third paper of this series (2).

These studies take into account both mechanisms of breakage: 1) splitting, as discussed in the previous section, and 2) surface erosion, as discussed in the Appendix. There are three parameters ($\tilde{k}$, σ_{ge}, ν_{ge}) in the surface erosion expression (Eq. A4). As starting values, σ_{ge} and ν_{ge} were taken from the literature (9) to be 3.5 and 1.5, respectively. Using the definition of sensitivity given by Eq. 33, the typical sensitivity values for ϕ_a, k_1, m, γ, $\tilde{k}$, and ϵ were found to be 2.7, 0.62, 1.4, 0.02, 0.001, and 10^{-6}, respectively. Thus, the parameters ϕ_a, k_1, and m were found overwhelmingly to be most sensitive. The value for γ was found to be less sensitive, and the values for $\tilde{k}$, ϵ, σ_{ge}, and ν_{ge} were found to be of least importance. This observation held true for both the continuous and discontinuous forms of breakage rate expression, $g(x)$. Therefore, both the aggregation and erosion terms were deleted from the original reversible model (Eq. 16) for the simulation of these particular disaggregation processes. Values for ϕ_a, k_1, m, and γ were searched for using the optimization routine. In some selected cases, the value of $\tilde{k}$ was varied to confirm that the erosion mechanism was not significant. The findings consistently suggest that the surface erosion mechanism does not play an important role in modeling the reversal of ADP-induced aggregation.

Case studies were carried out to establish the effects of ϕ_a, k_1, m, γ, and $\tilde{k}$ on the generated particle size distribution. In Fig. 5, the computed final condition with optimized values of the parameters is given by the open squares. Typical results for a 10% increase and decrease in ϕ_a are given by open circles and open triangles, respectively. A 10% increase in ϕ_a results in the formation of fragments with sizes less than 0.8 and a shift of the large aggregate peak to the left as shown in Fig. 5. Similar studies on the effect of k_1 and m gave very similar patterns of changes. In contrast, no noticeable change is observed for 10% changes in the parameters $\tilde{k}$ and γ (not shown).

DISCUSSION

A form of the population balance equation is developed in this paper for the purpose of describing the aggregation and

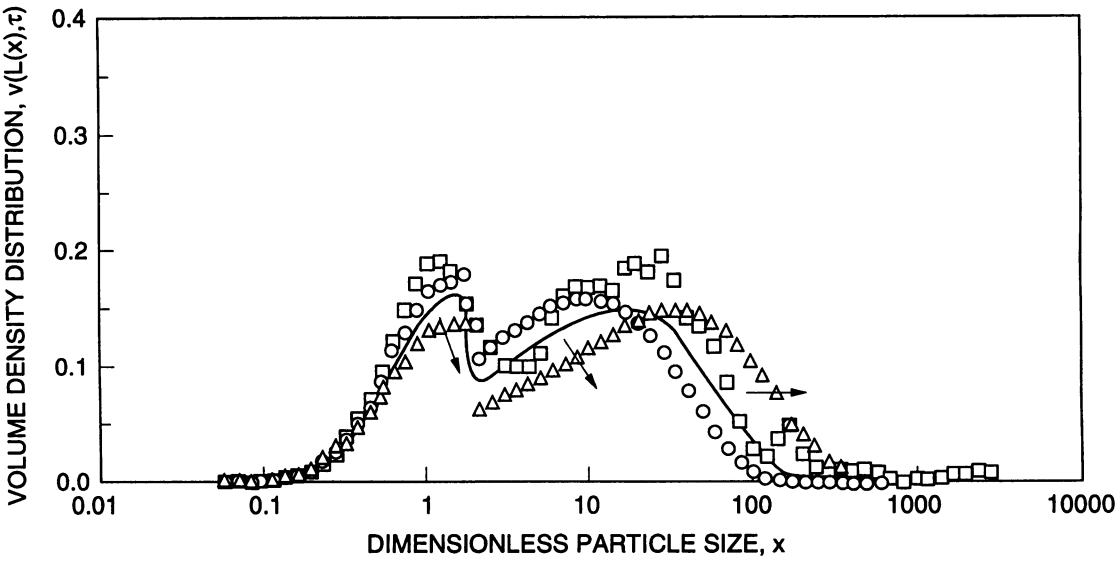

FIGURE 4 Effects of a ±10% perturbation on ϕ_a on the volume density distribution. (□) The histogram for the experimental data; (–) histogram for the computer-generated distribution with optimized values of ϕ_a, ϵ, and k_1 parameters; (△) histogram for the computer-generated distribution with a 10% increase in ϕ_a; and (○) histogram for the computer-generated distribution with a 10% increase in ϕ_a. All cases correspond to shear-induced aggregation of a platelet suspension (initial distribution not shown) for a time of 100 s at a shear rate of 5400 s^{-1}. The arrows show the direction of shift of the size distribution with increasing values of ϕ_a.

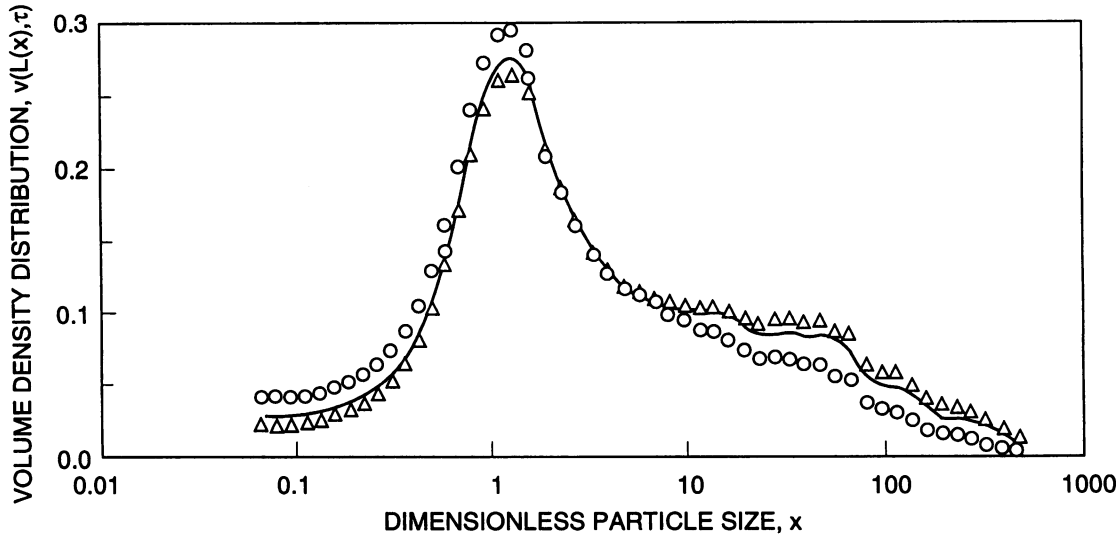

FIGURE 5 Effects of ±10% perturbation on ϕ_a on the volume density distribution. (–) Histogram for the computer-generated distribution with optimized values of ϕ_a, k_1, γ, m, and $\tilde{k}$ parameters; (○) histogram for the computer-generated distribution with a 10% increase in ϕ_a; (△) histogram for the computer-generated distribution with a 10% increase in ϕ_a; and (○) histogram for the computer-generated distribution with a 10% increase in ϕ_a. All cases correspond to shear-induced aggregation of a platelet suspension (initial distribution not shown) for a time of 100 s at a shear rate of 5400 s^{-1}. The arrows show the direction of shift of the size distribution with increasing values of ϕ_a. The distributions shown are at time of 60 s after the initial condition at which time extensive disaggregation has taken place.

disaggregation behavior of human blood platelets and platelet aggregates under the influence of the fluid mechanical shearing stress. Formulation of the aggregation expressions requires a relatively straightforward extension of the Smoluchowski coalescence kernel for aggregation of noninteracting hard spheres, as given by Eq. 19. Two parameters are introduced to account for 1) the fact that only a small fraction of particle collisions result in particle-particle binding, and 2) the effective collision diameter of aggregates is larger than compact spheres. A third parameter, Eq. 26, is required to account for fluid entrapment in aggregates.

Analytical solutions are not possible for the equation and initial conditions of interest in this work. Numerical methods are required. However, analytical solutions to the coalescence equation (aggregation without disaggregation) exist for certain simpler kernels and initial conditions. Studies

with these analytical solutions serve to validate the numerical procedure (Fig. 1), and serve to evaluate the applicability of several different forms of the coalescence kernel. The evaluations show that a somewhat simpler kernel $(x + y)$ gives very similar results to those of the Smoluchowski kernel $(x^{1/3} + y^{1/3})^3$, and these findings suggest a method of correlation of results for various values of the two coalescence parameters (Eq. 32).

Application of the model to analysis of experimental determinations of platelet aggregation induced by shear stress yield very good agreement between observed and calculated size distributions when the parameters of the model are selected appropriately (Fig. 4). Parameter sensitivity studies show that particle coalescence processes are of dominant importance in this case. Reversibility (disaggregation) processes can be neglected in shear-induced aggregation under the conditions studied.

Application of the model to analysis of experimental determinations of disaggregation under shear stress of platelet aggregates formed in response to low dosage ADP also yield good agreements. Disaggregation is inherently more complex than aggregation, and requires estimation of a number of parameters by use of prior work, and by use of parameter sensitivity studies. The sensitivity studies (Fig. 5) determine the relative importance of the parameters in numerical simulation of specific experiments with platelet suspensions. The results of these studies permit attention to be focused on the relatively few most important parameters. The sensitivity studies indicated that the key mechanism for disaggregation is aggregate splitting (the formation of several daughter fragments), rather than surface erosion. This finding permits important simplification of the model.

The result of this work is a mathematical simulation method for analysis of platelet aggregation and disaggregation reactions. The following two papers demonstrate the application of the method to the analysis of two cases of platelet response under the influence of fluid mechanical shear stress: 1) shear-induced aggregation, wherein coalescence processes are of dominant importance, and 2) disaggregation under shear stress of platelet aggregates previously formed in response to low dosage of ADP, wherein disaggregation processes are of dominant importance.

NOMENCLATURE

Roman symbols

F	objective function in nonlinear least minimization routine
$g(v)$	breakage frequency, s^{-1}
G	shear rate, s^{-1}
$Q(v)$	the instantaneous rate of change of the volume of parent particle of size v, μm^{-3} s^{-1}
h	ratio of net volume/gross volume
H	limiting value of h for large aggregates
$\tilde{k}$	erosion rate constant, dimensionless
k_1	breakage rate constant in Eq. 4, s^{-1}
k_2	empirical coefficient in Eq. 8, dimensionless
k_3	empirical coefficient in Eq. 7, dimensionless
$k_G(v,w)$	continuous coalescence kernel
$L(x)$	dimensionless logarithmic scale
m	order of breakage rate, dimensionless
$n_{cal}(x,\tau)$	calculated number density distribution
$n(v,t)$	differential particle number concentration distribution, μm^{-3} cm^{-3}
p	empirical coefficient (Eq. 8), dimensionless
P	total dimensionless particle population
$p_s(v,w)$	fragment size distribution due to breakage or disaggregation, μm^{-3}
P_e	distribution of erosion fines, μm^{-3}
q	empirical coefficient (Eq. 7), dimensionless
q_e	total rate of formation of erosion fines of all sizes,/ eroding particle of size w
v,w	particle volume, μm^3
v,w	mean daughter volume size due to breakage, μm^3
v_o	average particle volume of initial particle suspension, μm^3
$v_{cal}(x,\tau)$	calculated volume density distribution
v_e	mean erosion volume, μm^3
v_{ge}	geometric volume, μm^3
v_i	particle volume consists of i singlets, μm^3
v_s	volume of the smallest particle, μm^3
v_{ss}	maximum stable size before breakage, μm^3
x, y	dimensionless particle volumes, v/v_o and w/v_o, respectively (the number of particles in an aggregate)
x_s	smallest dimensionless particle in suspension at time zero
x_{ss}	maximum stable size before breakage, dimensionless

Greek symbols

Γ	gamma function
γ	average number of fragments formed by breakage, dimensionless
ϵ	collision efficiency
ξ	estimate of the population parameters near the minimum of F
σ	standard deviation of fragment size distribution due to breakage, μm^3
σ_e	arithmetic standard deviation of erosion product distribution, μm^3
σ_{ge}	geometric standard deviation, dimensionless
τ	dimensionless time
ϕ	void fraction (related to collision diameter), dimensionless, Eq. 19
ϕ_a	void fraction parameter defined in Eq. 19

APPENDIX: EQUATIONS FOR DISAGGREGATION BY SURFACE EROSION

The erosion processes continuously reduce the size of the parent aggregates in the system. The net contribution to the rate of change of the number concentration on the size interval $(v,v + dv)$ is obtained by balancing the rates at which particles enter and leave the interval as they continuously shrink. If $n(v,t)dv$ is the number of particles in the interval, and $\partial(n(v,t)dv)/\partial t$ is the rate of accumulation of number of particles in the finite interval, then (following the development of Pandya and Spielman (9, 10)):

$$\frac{\partial n(v,t)}{\partial t}dv = -\frac{\partial}{\partial v}[Q(v)n(v)]dv. \quad \text{(A1)}$$

Here $Q(v) = dv/dt$ is the instantaneous rate of change of the volume of a parent particle of size v. As erosion occurs, the lost material reappears as

erosion daughter fragments. The probability of erosion fines in the interval due to erosion of parent aggregates of size $w>v$ is given by

$$\frac{P_e(v)dv}{\int_0^w P_e(v')\,dv'}. \tag{A2}$$

The rate of accumulation due to formation of erosion fragments of size v is then given by

$$\frac{P_e(v)dv \int_v^\infty q_e(w)n(w,t)\,dw}{\int_0^w P_e(v')\,dv'} \tag{A3}$$

where q_e is total rate of formation of erosion fines of all sizes, per eroding particle of size w; and P_e is the distribution of erosion fines. To account for particle breakage by surface erosion, Eqs. A1 and A3 are added to the right hand side of Eq. 1 to give the final form of the population balance equation. These two terms represents the net rate of change of parent particles of size v due to erosion and the rate of production of fine particles by erosion.

Assumption of a lognormal erosion particle size distribution leads to expressions for $Q(v)$ and q_e:

$$Q(v) = \tilde{k}Gv_e \left\{ \frac{1 + \text{erf}\left[\frac{\ln\left(\frac{v}{v_{ge}}\right)}{\sqrt{2}\ln\sigma_{ge}} - \frac{\ln\sigma_{ge}}{\sqrt{2}} \right]}{1 + \text{erf}\left[\frac{\ln\left(\frac{v}{v_{ge}}\right)}{\sqrt{2}\ln\sigma_{ge}} \right]} \right\} \tag{A4}$$

$$q_e = \tilde{k}G \tag{A5}$$

where $\tilde{k}$ is the erosion rate coefficient, erf(x) is the error function, and v_{ge} (geometric mean) and σ_{ge} (geometric mean standard deviation) are related by Eqs. A6 and A7 as follows.

$$v_{ge} = \frac{v_e}{\sqrt{\ln\left[1 + \left(\frac{\sigma_e}{v_e}\right)^2\right]}} \tag{A6}$$

$$\ln\sigma_{ge} = \sqrt{\ln\left[1 + \left(\frac{\sigma_e}{v_e}\right)^2\right]} \tag{A7}$$

REFERENCES

1. Huang, P. Y., and J. D. Hellums. 1992. Aggregation and disaggregation kinetics of human blood platelets. II. Shear-induced platelet aggregation. *Biophys. J.* 65:344–353.
2. Huang, P. Y., and J. D. Hellums. 1992. Aggregation and disaggregation kinetics of human blood platelets. III. Reversal Phase of ADP-Induced Platelet Aggregation. Biophys. J. 65:354–361.
3. Drake, R. L. 1972. A general mathematical survey of the coagulation equation. *In* Topics in Current Aerosol Research. G. M. Hidy and J. R. Brocks, editors. Pergamon Press, Oxford. pp. 203–384.
4. Belval, T. K., and J. D. Hellums. 1986. Analysis of shear-induced platelet aggregation with population balance mathematics. *Biophys. J.* 50: 479–487.
5. Melzak, Z. A. 1957a. A scalar transport equation. *Trans. Am. Math. Soc.* 85:547–560.
6. Melzak, Z. A. 1957b. A scalar transport equation II. *Mich. Math. J.* 4:193–206.
7. Valentas, K. J., and N. R. Amundson. 1966. Breakage and coalescence in dispersed phase system. *Ind. Eng. Chem. Fund.* 5:533–542.
8. Valentas, K. J., O. Bilous, and N. R. Amundson. 1966. Analysis of breakage in dispersed phase systems. *Ind. Eng. Chem. Fund.*, 5:271–279.
9. Pandya, J. D., and L. A. Spielman. 1983. Floc breakage in agitated suspensions: Effect of agitation rate. *Chem. Eng. Sci.* 38:1983–1992.
10. Pandya, J. D., and L. A. Spielman. 1982. Floc breakage in agitated suspension: Theory and data processing strategy. *J. Colloid. Int. Sci.* 90:517–531.
11. Smoluchowski, M. V. 1917. Versuch einer mathematischen theorie der koagulationskinetic kolloider losunger. *Z. Physik. Chem.* 92:129–168.
12. Huang, P. Y. 1991. The kinetics of human platelet aggregation and disaggregation in controlled shear field. Ph.D. thesis. Rice University. 233 pp.
13. Austin, L. G. 1971. A review: Introduction to the mathematical description of grinding as a rate process. *Powder Technol.* 5:1–17.
14. Ramkrishna, D., and J. D. Borwanker. 1974. A puristic analysis of population balance II. *Chem. Eng. Sci.* 29:1711–1721.
15. Ray, D. T., and R. Hogg. 1987. Agglomerate breakage in polymer-flocculated suspensions. *J. Colloid. Int. Sci.* 116:256–268.
16. Peterson, T. W. 1986. Similarity solutions for the population balance equation describing particle fragmentation. *Aerosol Sci. Technol.* 5:93–101.
17. Berry, E. X. 1967. Cloud droplet growth by collection. *J. Atmos. Sci.* 24:688–701.
18. Frojmovic, M. M., M. Newton, and H. L. Goldsmith. 1976. The microrheology of mammalian platelets: Studies of rheo-optical transients and flow in tubes. *Microvasc. Res.* 11:203–215.
19. Born, G. V. R., and R. Hume. 1967. Effects of numbers and sizes of platelet aggregates on the optical density of plasma. *Nature (Lond.)* 215:1027–1029.
20. Karino, T., and H. L. Goldsmith. 1979. Aggregation of human platelets in an annular vortex distal to tubular expansion. *Microvasc. Res.* 17: 217–237.
21. Chang, H. N., and C. R. Robertson. 1976. Platelet aggregation by laminar shear flow and Brownian motion. *Ann. Biomed. Eng.* 4:151–183.
22. Bell, D. N., and H. L. Goldsmith. 1984. Platelet aggregation in Poiseuille flow: Effect of shear rate. *Microvasc. Res.* 27:316–330.
23. Lu, C. F., and L. A. Spielman. 1984. Kinetics of breakage and aggregation in agitated liquid suspensions. *J. Colloid. Int. Sci.* 103:95–105.
24. Nelder, J. A., and R. Meads. 1965. A Simplex method for function minimization. *Comp. J.* 7:308–316.
25. Latimer, P. 1983. Blood platelet aggregometer: Predict effects of aggregation, photometer geometry, and multiple scattering. *Applied Optics* 22:1136–1143.
26. Scott, W. T. 1965. Analytical studies of cloud droplet coalescence I No. DRI Tech. Rep. 9. University of Nevada, Reno, NV. 72 pp.
27. Spiegel, M. R. 1968. Mathematical Handbook of Formulas and Tables. McGraw-Hill Book Company, New York. 271 pp.